Predicting Vibrational Mean Free Paths in Disordered Systems

Jason M. Larkin,[1] Joseph E. Turney,[1] Alexandre D. Massicotte,[1] Cristina H. Amon,[1,2] and A. J. H. McGaughey[3,*]

[1]*Department of Mechanical Engineering*

Carnegie Mellon University

Pittsburgh, PA 15213

[2] *Department of Mechanical & Industrial Engineering,*

University of Toronto, Toronto, Ontario, Canada M5S 3G8

[3]*Department of Mechanical Engineering*

Carnegie Mellon University

Pittsburgh, PA 15213

(Dated: September 18, 2012)

Abstract

I. INTRODUCTION

The goal of this work is to predict

II. DETERMINING PROPAGATING AND LOCALIZED MODES

Klemens scattering paper showing rayleigh[?] .

Duda shows the reduction in group velocity of disordered systems.[?]

Garg show that the virtual crystal approximation works well for Si-Ge[?]

Duda shows that taking a perfect alloy and disordering via an order parameter allows control of thermal conductivity.[?]

Tamura gives an expression for mass defect scattering which is harmonic and given by[?] : The Rayleigh scattering limit is observed in the low-frequency limit, where the DOS is approximately Debye.

Cahill shows that conductivty of Ge-doped Si epitaxial layers agrees with the defect scaling cross section is captured mostly by the mass disorder.[?]

Cahill shows that even though the mass difference between Si and Ge is larger than the mass of Si, the defect scaling agrees with experimental measurements of thermal conductivity in dilute SiGe epitaxial layers.[?]

Tian showed, using ab initio calculations, that the virtual crystal appromxation with defect scalings work well for predicting the thermal conductivity of PbSe/PbTe alloys.[?]

Bouchard show that alloy DOS varies smoothly with concentration.[?]

III. THERMAL CONDUCTIVITY PREDICTIONS FROM MOLECULAR DYNAMICS

The thermal conductivity of amorphous solids at low temperatures contain quantum statistical effects.[?] Molecular dynamics simulations are not able to capture quantum statistical effects.

IV. KINETIC THEORY

k = sum over modes

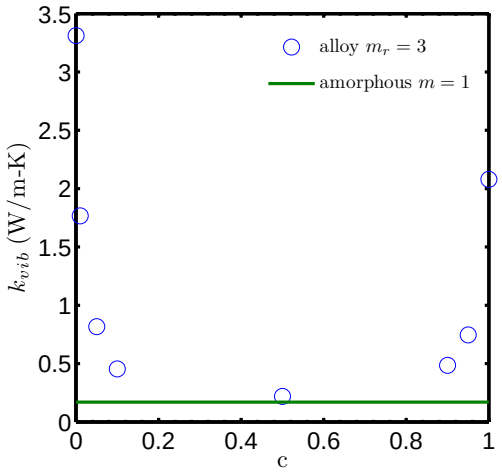

FIG. 1: The vibrational conductivity of LJ alloys predicted using MD simulations and the Green-Kubo method. The predicted thermal conductivities are for a LJ alloy of the form $m^a_{1-c}m^b_c$, where $m^a = 1$, $m^b = 3$, and $m_r = m^a/m^b = 3$ (in LJ units). As the alloy concentration is increased perturbatively, the vibrational conductivity drops quickly and saturates to a minimum at $c = 0.5$. For $c = 0.5$ the system is heavily disordered and the vibrational conductivity approaches that of an amorphous system.

For a perfect system, all vibrational modes are phonons. It is thus easy to evaluate.

Diffusons, locons and propagons[?] .

$$k_{vib,\mathbf{n}} = \sum_{\boldsymbol{\kappa}} \sum_{\nu} c_{ph}(\boldsymbol{\kappa}_\nu)\, \boldsymbol{v}^2_{g,\mathbf{n}}(\boldsymbol{\kappa}_\nu)\, \tau(\boldsymbol{\kappa}_\nu)\,. \tag{1}$$

$$\Lambda(\boldsymbol{\kappa}_\nu) = |\boldsymbol{v}_g|\tau(\boldsymbol{\kappa}_\nu)\,, \tag{2}$$

V. PHONON LIFETIMES

$$\frac{1}{\tau} = \frac{1}{\tau_{p-p}} + \frac{1}{\tau_b} + \frac{1}{\tau_d}, \tag{3}$$

where τ_{p-p} accounts for phonon-phonon scattering, τ_b accounts for boundary scattering, τ_d accounts for defect scattering.

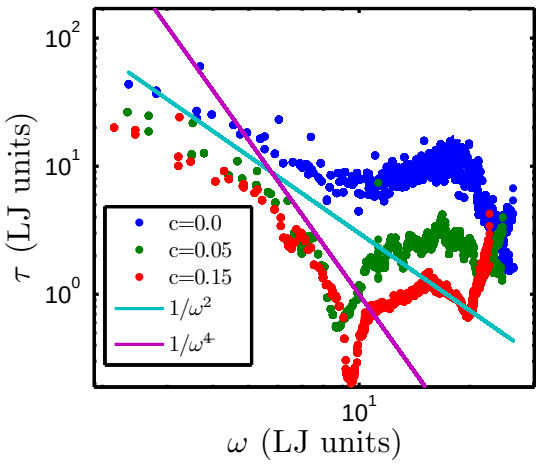

FIG. 2: virtual crystal results

$$\tau_{p-p} = \frac{(6\pi^2)^{1/3}\bar{m}v_g v_p^2}{2V^{1/3}\omega^2\gamma^2 T}, \tag{4}$$

$$\frac{1}{\tau_d} = \frac{V\omega^4}{4\pi v_p^2 v_g}(\sum_i c_i(1 - m_i/\bar{m})^2 + \sum_i c_i(1 - r_i/\bar{r})^2), \tag{5}$$

where c_i is the fraction, m_i is the mass, and r_i is the radius of species i and $\bar{r}$ is the average atomic radius.[? ?] The frequency dependence is the same as Rayleigh scattering, where high frequency modes are scattered most strongly.

$$\tau_b = L/v_g. \tag{6}$$

Boundary scattering is responsible for decreasing the long lifetimes (mean free paths) of low frequency phonons which carry a significant amount of heat, making it particularly effective at decreasing the thermal conductivity of systems with length scale of 100s of μm and less.[?]

- compare lifetimes from 2 atom alloy, 4 atom alloy. Is the reduction in thermal conductivity mostly due to the reduction in group velocities/introduction of optical modes?

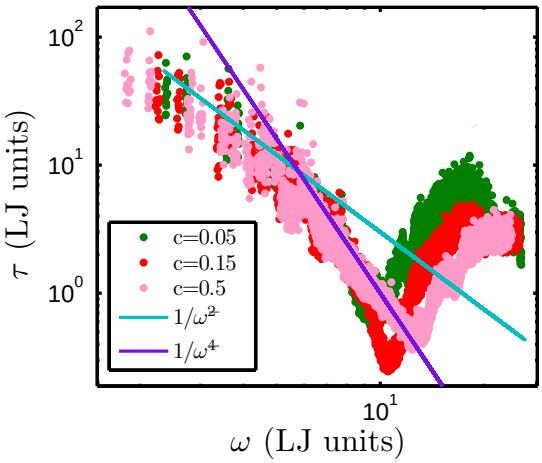

FIG. 3: gamma point results

A. Virtual Crystal Approximation

B. Bond Disorder

The decreased vibrational conductivity of systems which are highly anharmonic, such as weak covalently and Van der Waals bonded systems,? is accounted for by the Gruneisen parameter. For a purely harmonic system, the mode specific Gruneisen parameter is zero and the phonon lifetimes are infinite.

$$\frac{1}{\tau_d} = \frac{\pi}{2N}\omega^2(\boldsymbol{\kappa}_\nu) \sum_{\boldsymbol{\kappa}',\nu'}^{N,3n} \delta(\omega(\boldsymbol{\kappa}_\nu) - \omega(\boldsymbol{\kappa}'_{\nu'})) \sum_{b}^{n} g(b) |e^*(\boldsymbol{\kappa}_\nu\ {}^{b}_{\alpha})\, \dot{e}(\boldsymbol{\kappa}_\nu\ {}^{b}_{\alpha})\,|^2, \tag{7}$$

$g(b) = \sum_i f_i(b)[1 - m_i(b)/m_{avg}(b)]^2$

C. Mass Disorder

why not bond disorder? This has been investigated such as in Schelling Si/Ge? , where it was shown that mass disorder is the dominant scattering mechanism. Also, a first principle study of Si/Ge demonstrates that virtual crystal approxmation Marzari Si/Ge PRL? . Although, detailed study of PbTe/PbSe systems demonstrate the importance of bond environment for alloys.?

D. Group Velocity

The reduced vibrational conductivity of germanium compared to silicon can be explained in both in terms of the $\bar{m}$ (germanium has a larger density ρ than silicon) and the group velocity (germanium has a smaller bulk modulus B, and $v_g \propto \sqrt{B/\rho}$.

- $v_g(m_r)$
- two masses with $v_g(m_r)$, maybe compare with 4 masses with higher mass ratio.
- Keep m_{avg} constant for all.
- run a system with a "softer" and "stiffer" LJ (smaller/bigger eps or sigma). This can be used as a comparison for the phonon/diffuson spectrums which will be shown later.

Appendix A: Predicting Vibrational Lifetimes

1. Vibrations in Ordered and Disordered Solids

In a crystal (periodic) system, the vibrations of atoms are described by a basis of eigenfunctions called phonon normal modes, which are determined by the properties of the crystal (see Appendix A 3). The eigenvalues of this basis are the phonon mode frequencies (energies).[? ?] The atomic velocities can be represented by the velocity normal mode coordinate, defined as[?]

$$\dot{u}_\alpha(\tbinom{l}{b};t) = \sum_{\boldsymbol{\kappa}',\nu}^{N,3n} \frac{1}{\sqrt{m_b N}} \exp\Big[i\boldsymbol{\kappa}' \cdot \mathbf{r}_0(\tbinom{l}{0})\Big] e^*(\tbinom{\boldsymbol{\kappa}}{\nu}\ \tbinom{b}{\alpha})\, \dot{q}(\tbinom{\boldsymbol{\kappa}}{\nu};t)\,. \tag{A1}$$

Here, $\dot{q}(\tbinom{\boldsymbol{\kappa}}{\nu};t)$ represents the kinetic energy $T(\tbinom{\boldsymbol{\kappa}}{\nu};t)$ of the mode with phonon frequency $\omega_0(\tbinom{\boldsymbol{\kappa}}{\nu})$ by[?]

$$T(\tbinom{\boldsymbol{\kappa}}{\nu};t) = \frac{\dot{q}^*(\tbinom{\boldsymbol{\kappa}}{\nu};t)\,\dot{q}(\tbinom{\boldsymbol{\kappa}}{\nu};t)}{2}. \tag{A2}$$

The phonon mode kinetic energies $T(\tbinom{\boldsymbol{\kappa}}{\nu};t)$ are used to calculate the phonon spectral energy denisty in Appendix A 2.

2. Allowed Wavevectors in Ordered Systems

The phonon spectral energy is defined for the allowed wavevectors of a crystal, which can be specified from the crystal structure's Bravais lattice and its basis, i.e. unit cell. A

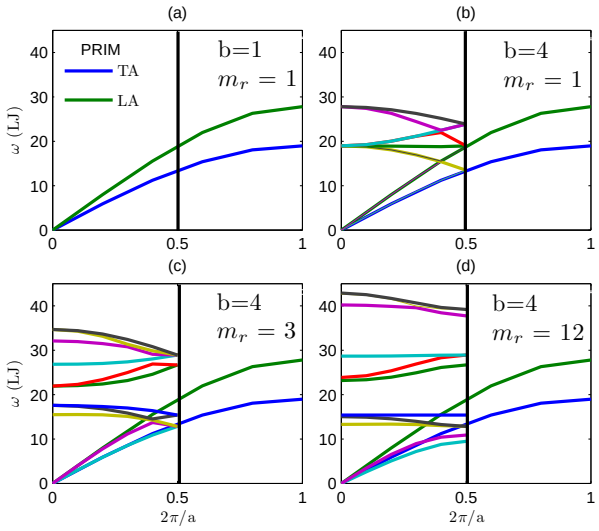

FIG. 4: Dispersion plots for Lennard-Jones systems with varying number of atoms in the unit cell ($b = 1..4$) and mass ratio (m_r) for wavevectors in the direction $2\pi/a[100]$. (a) Dispersion plot using the FCC primitive unit cell ($b = 1$), which shows that only acoustic phonon branches exist in the system. The edge of the Brillouin zone in this direction is $2\pi/a[100]$. (b) Dispersion plot using the cubic conventional unit cell ($b = 4$), where every atom in the unit cell is identical ($m_r = 1$). Compared to the primitive cell, the Brillouin zone edge is at $\pi/a[100]$ where the acoustic branches have been "folded in".[?] Other than these considerations, the choice of unit cell for the single species system does not affect the dispersion. (c) System with two unique atom types in the conventional unit cell with a mass ratio $m_r = 3$, which creates optical branches with low group velocity and reduced group velocity acoustic branches. (d) System with $b = 4$ unique atoms types in the unit cell with high mass ratio ($m_r = 12$), which increases the number of optical branches and further reduces the acoustic group velocities.

D-dimensional Bravais lattice is a collection of points with positions

$$\mathbf{u}_0\binom{l}{0} = \sum_{\alpha}^{D} N_\alpha \mathbf{a}_\alpha \tag{A3}$$

where N_α and the summations if over the lattice vectors, $\mathbf{a}_\alpha$.[?] The basis (or unit cell) is the building block of the crystal and they are arranged on the points defined by the Bravais lattice. The equillibrium position of any atom in the crystal can be described by

$$\mathbf{u}_0\binom{l}{b} = \mathbf{u}_0\binom{l}{0} + \mathbf{u}_0\binom{0}{b} \tag{A4}$$

where $\mathbf{u}_0\binom{l}{0}$ is the equilibrium position of the l^{th} unit cell and $\mathbf{u}_0\binom{0}{b}$ is the equilibrium position of the and b^{th} atom in the unit cell relative to $\mathbf{u}_0\binom{l}{0}$. For the LJ systems studied here, the cubic conventional cells are used with four atoms per unit cell.[?] For our MD simulations, cubic simulation domains with periodic boundary conditions are used with $N_1 = N_2 = N_3 = N_0$.[? ?] The allowed wavevectors for such crystal structures are

$$\boldsymbol{\kappa} = \sum_{\alpha} \mathbf{b}_\alpha \frac{n_\alpha}{N_\alpha}, \tag{A5}$$

where $\mathbf{b}_\alpha$ are the reciprocal lattice vectors[?] and $-N_\alpha/2 < n_\alpha \leq N_\alpha/2$, where n_α are integers and N_α are even integers.[?] The wavevectors are taken to be in the first Brioullin zone.[?]

Allowed Wavevectors in Disordered Materials

Strictly speaking, the only allowed wavector in a disordered system is the gamma point ($\kappa = [000]$). As such, the lattice dynamics calculations are performed at the gamma point:

3. Normal Mode Decomposition

Normal mode decomposition and its limitations.[?]

If $\gamma\binom{\boldsymbol{\kappa}}{\nu} > \omega\binom{\boldsymbol{\kappa}}{\nu}$, then the vibrational mode is overdamped. Discuss why real-space method is necessary in this case.

4. Thermal Conductivity

Once the lifetimes (MFPs) and group velocities of all virbrational modes in the Brillouin zone are obtained, the bulk thermal conductivity in direction $\mathbf{n}$, $k_\mathbf{n}$, can be calculated from[?]

$$k_\mathbf{n} = \sum_{\boldsymbol{\kappa}} \sum_{\nu} c_{ph}\binom{\boldsymbol{\kappa}}{\nu} \, v^2_{g,\mathbf{n}}\binom{\boldsymbol{\kappa}}{\nu} \, \tau\binom{\boldsymbol{\kappa}}{\nu} . \tag{A6}$$

Here, c_{ph} is the phonon volumetric specific heat and $v_{g,\mathbf{n}}$ is the component of the group velocity vector in direction $\mathbf{n}$. Since the systems we consider are classical and obey Maxwell-Boltzmann statistics,[?] the specific heat is k_B/V per mode in the harmonic limit where V is the system volume. This approximation is used here and has been shown to be suitable for LJ argon[?] and SW silicon.[?] The group velocity vector is the gradient of the dispersion

FIG. 5: Thermal conductivity predictions for LJ argon calculated using phonon lifetimes predicted by Φ and Φ'.[?] (a) The finite simulation-size scaling extrapolation[? ?] is used to compare the results to bulk predictions made using the Green-Kubo method. (b) The bulk results for Φ and Green-Kubo are in good agreement temperatures of 20 and 40 K with those of other atomistic simulation methods.[?]

curves (i.e., $\partial\omega/\partial\boldsymbol{\kappa}$), which can be calculated from the frequencies and wavevectors using finite differences. In this work, the group velocities are calculated using finite difference and quasi-harmonic lattice dynamics because a very small finite difference can be used which reduces the error.[?] To predict a bulk thermal conductivity, it is necessary to perform a finite simulation size scaling procedure as discussed in Appendix B.

Appendix B: Finite Simulation-Size Scaling for Thermal Conductivity

For the LJ argon system studied in Section **??**, a finite simulation-size scaling procedure[? ?] is used to compare the thermal conductivity predictions from Φ and Φ' to those from the Green-Kubo method. The scaling procedure is demonstrated in Fig. 6. The thermal conductivity is predicted from Φ or Φ' and MD simulations with $N_0 = 4, 6, 8$, and 10. The bulk conductivity, k_∞, is then estimated by fitting the data to

$$1/k = 1/k_\infty + A/N_0, \tag{B1}$$

where A is a constant. This procedure is necessary because the first Brillouin zone is only sampled at a finite number of points for a finite simulation size, with no contribution from the volume at its center. To predict a bulk thermal conductivity, it is important to sample points near the Brillouin zone center, where the modes can have large lifetimes and group velocities.[? ?]

* Electronic address: mcgaughey@cmu.edu

P. G. Klemens, Proceedings of the Physical Society. Section A **68**, 1113 (1955), URL http://stacks.iop.org/0370-1298/68/i=12/a=303.

J. C. Duda, T. S. English, D. A. Jordan, P. M. Norris, and W. A. Soffa, Journal of Physics: Condensed Matter **23**, 205401 (2011), URL http://stacks.iop.org/0953-8984/23/i=20/a=205401.

J. Garg, N. Bonini, B. Kozinsky, and N. Marzari, Phys. Rev. Lett. **106**, 045901 (2011), URL http://link.aps.org/doi/10.1103/PhysRevLett.106.045901.

J. C. Duda, T. S. English, D. A. Jordan, P. M. Norris, and W. A. Soffa, Journal of Heat Transfer **134**, 014501 (2012).

S.-i. Tamura, Phys. Rev. B **27**, 858866 (1983), URL http://link.aps.org/doi/10.1103/PhysRevB.27.858.

D. G. Cahill and F. Watanabe, Phys. Rev. B **70**, 235322 (2004), URL http://link.aps.org/doi/10.1103/PhysRevB.70.235322.

D. G. Cahill, F. Watanabe, A. Rockett, and C. B. Vining, Phys. Rev. B **71**, 235202 (2005), URL http://link.aps.org/doi/10.1103/PhysRevB.71.235202.

Z. Tian, J. Garg, K. Esfarjani, T. Shiga, J. Shiomi, and G. Chen, Phys. Rev. B **85**, 184303 (2012), URL http://link.aps.org/doi/10.1103/PhysRevB.85.184303.

A. M. Bouchard, R. Biswas, W. A. Kamitakahara, G. S. Grest, and C. M. Soukoulis, Phys. Rev. B **38**, 1049910506 (1988), URL http://link.aps.org/doi/10.1103/PhysRevB.38.10499.

J. J. Freeman and A. C. Anderson, Physical Review B **34**, 5684\textbackslash965690 (1986).

P. B. Allen, J. L. Feldman, J. Fabian, and F. Wooten, Philosophical Magazine B **79**, 1715 (1999).

P. G. Klemens, Proceedings of the Physical Society. Section A **70**, 833 (1957), URL http://stacks.iop.org/0370-1298/70/i=11/a=407.

A. J. H. McGaughey and A. Jain, Applied Physics Letters **100**, 061911 (2012), URL http://link.aip.org/link/?APL/100/061911/1.

A. Skye and P. K. Schelling, Journal of Applied Physics **103**, 113524 (2008), URL http://link.aip.org/link/?JAP/103/113524/1.